

Hybrid integrated ultra-low linewidth coil stabilized isolator-free widely tunable external cavity laser

David A. S. Heim¹, Debapam Bose¹, Kaikai Liu¹, Andrei Isichenko¹, and Daniel J. Blumenthal^{1*}

¹ Department of Electrical and Computer Engineering, University of California Santa Barbara, Santa Barbara, CA, USA

* danb@ucsb.edu

ABSTRACT

Precision applications such as quantum computing, quantum and fiber sensing, and mmWave and RF generation, require ultra-low phase noise stabilized lasers operating at wavelengths across the visible to near-IR. These applications employ widely tunable table-scale laser systems, bulk-optic reference cavities, and optical isolation to achieve ultra-low frequency noise and high stability across wide wavelength ranges. Photonic integration promises to bring these laser systems to the chip-scale, enabling reliable, scalable and portable precision applications. Here we report record-low integrated laser linewidths with a coil-cavity stabilized 1550 nm tunable laser, that achieves 3 to 7 Hz fundamental linewidth across a 60 nm tuning range and 27 – 60 Hz integral linewidths with an Allan deviation of 1.8E-13 at 6.4 ms across 40 nm. These results represent 5-orders of magnitude noise reduction and almost 2-orders magnitude reduction in integral linewidth for widely tunable integrated lasers. The hybrid integrated silicon nitride external cavity tunable laser is stabilized to a silicon nitride 10-meter long integrated coil-resonator without the need for an optical isolator by leveraging the inherent 45 dB isolation. The laser and reference cavity are fabricated in the same 80 nm-thick ultra-low loss Si₃N₄ waveguide CMOS foundry compatible process, which combined with the inherent isolation, unlocks the path towards fully integrated visible to NIR frequency-stabilized lasers.

INTRODUCTION

Ultra-narrow linewidth stabilized lasers are critical for a wide range of precision applications including optical atomic clocks¹⁻³, quantum computing^{4,5}, metrology⁶, quantum and fiber sensing⁷⁻¹¹, low phase noise mmWave and RF generation^{12,13}, and space-based applications. Of paramount importance to these applications is the phase noise as measured from low to high carrier offset frequencies and characterized in part by the instantaneous and integral linewidths. To achieve ultra-low instantaneous and integral linewidths, these lasers systems utilize large mode volume lab-scale external cavity lasers and bulk-optic reference cavities^{14,15} and optical isolation in the laser stabilization circuit. Integration using a broadly transparent platform without the need for optical isolation will improve reliability, reduce size, weight, power, and cost, and enable scalability, portability, and systems-on-chip solutions across the visible to near-IR (NIR) and eventually down to the UV. Yet, to date, integration of widely tunable, cavity stabilized lasers, in a CMOS foundry compatible integrated platform, has remained elusive. Low instantaneous linewidth lasers include self-injection locked (SIL)¹⁶⁻¹⁹, stimulated Brillouin scattering (SBS)²⁰⁻²², external cavity DBR²³, and external cavity lasers (ECLs)^{24,25}. In particular, the external cavity tunable laser (ECTL) design is widely used due to its wide wavelength tuning range, low instantaneous linewidth, and ability to stabilize the laser output to an external optical reference cavity for integral linewidth reduction and carrier stabilization. Photonic integration of stabilized ECTLs is a critical step forward for robust laser solutions, operating from the visible to IR, to serve as stand-alone sources and as pumps for other laser types such as Brillouin lasers.

The ultra-low loss silicon nitride (Si_3N_4) platform²⁶ is ideal for integration of a widely tunable frequency stabilized ECTL due to the ultra-low waveguide propagation losses that extends from the visible to IR. The combination of ultra-high Q resonators^{27,28}, large mode volume coil reference cavities^{29,30}, the ability to integrate gain media, waveguide-compatible tuning, control, and modulation³¹⁻³³ enable a wide range of systems-on-chip solutions³⁴. To date silicon nitride photonics has been successfully used to realize large mode-volume resonator reference cavities³⁵⁻³⁷ and narrowly tunable low fundamental linewidth lasers³⁸⁻⁴¹. The high Q resonators enable increased intra-cavity photon lifetime and photon number needed to reduce the fundamental linewidths, while large mode-volume laser and reference cavities decrease intrinsic noise sources such as thermorefractive noise (TRN)^{30,42}. Additionally, a high laser resonator Q can improve the resilience to optical feedback^{24,43}. Hybrid integration of Si_3N_4 ECTLs⁴⁴⁻⁴⁸ is an effective way to combine the benefits of ultra-low loss waveguides and high Q resonators with III-V semiconductor gain materials at a wide range of wavelengths from the visible to IR. However, to date, achieving both low fundamental and integral linewidths, across widely tunable wavelength ranges, without the need for optical isolation, in a common integration platform that supports the ECTL, reference cavity, and other photonic components, has not been achieved.

Here we present a major advance in chip-scale widely tunable stabilized laser technology by demonstrating an isolator-free hybrid integrated Si_3N_4 external cavity tunable laser (ECTL) with

a wide 60 nm tuning range, stabilized to a 10-meter long Si_3N_4 integrated coil-resonator reference cavity. We report record-low fundamental linewidth (FLW) of 3 to 7 Hz across a full 60 nm tuning range with greater than 65 dB side mode suppression ratio. By directly locking, without optical isolation, the ECTL to a 10-meter long silicon nitride integrated coil resonator, we achieve record-low 27 - 60 Hz $1/\pi$ integral linewidth (ILW) across a 40 nm tuning range, a reduction of 65x from free-running. The low 20 MHz free-spectral range (FSR) of the 10-meter coil cavity enables frequency locking and stabilization at almost any wavelength across the tuning range within the FSR. The free running laser frequency noise is reduced by 5 orders of magnitude and we measure a record-low, to the best of our knowledge, Allan deviation (ADEV) of 1.8×10^{-13} at 6.4 ms, and 5.0 kHz/s drift. An accurate ILW measurement is achieved using a stabilized frequency comb noise characterization tool that measures down to 1 Hz frequency offset across a 40 nm tuning range. We demonstrate that the feedback resilience of the 3.5 million intrinsic-Q Vernier rings in the ECTL provide an inherent isolation of ~ 45 dB relative to a typical commercial III-V DFB laser (see Methods). Both the ECTL and 10-meter coil-reference cavity are fabricated in the same 80 nm thick silicon nitride low loss platform. This common integration combined with the inherent optical isolation of the ECTL enables a path towards full integration of widely tunable, narrow-linewidth, frequency stabilized lasers at a wide range of quantum, atomic, fiber communication, and other wavelengths from the visible through the NIR.

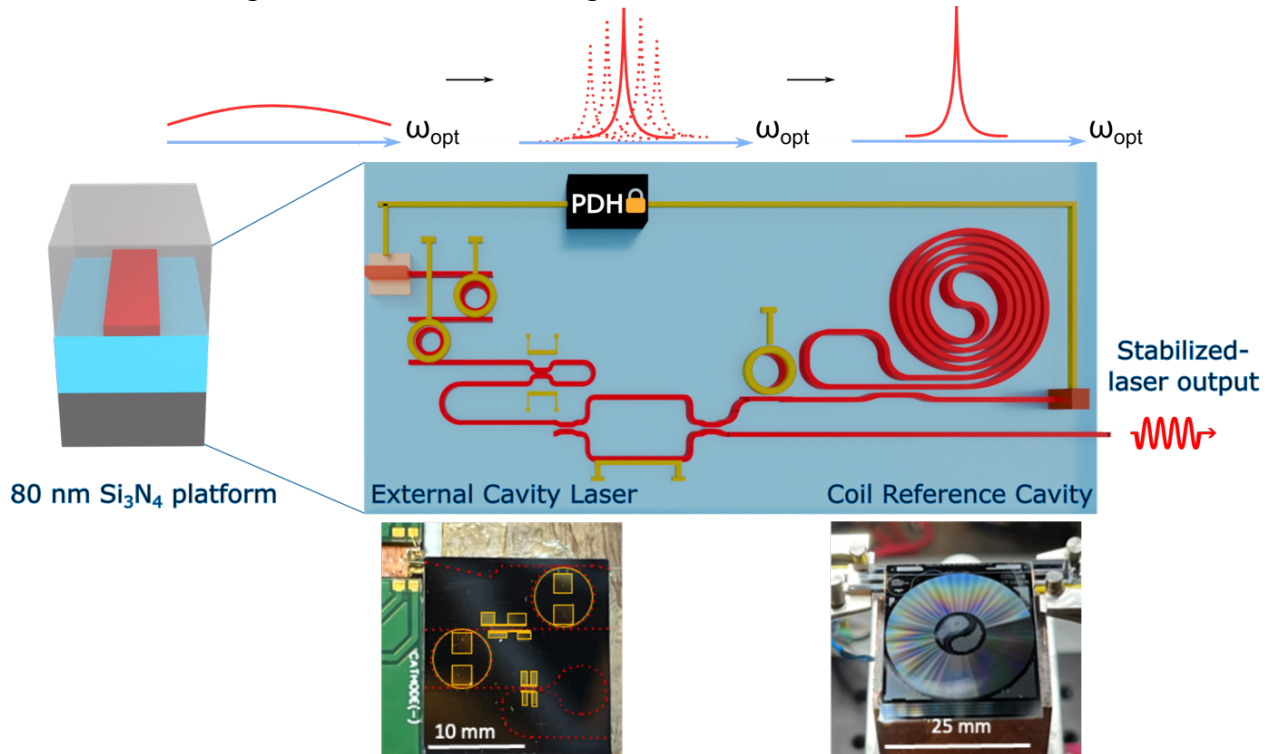


Fig. 1 Vision illustration of integrated coil-resonator stabilized hybrid integrated isolator free ECTL. Example of how the hybrid-integrated silicon nitride external cavity tunable laser (ECTL) (shown in image, bottom left) can be combined, on the same chip, with the integrated silicon nitride coil resonator reference cavity (shown in image, bottom right) designed in the same 80 nm thick Si_3N_4 platform. Hybrid integration of an RSOA provides a gain element (top

left), the high-Q Si_3N_4 rings serve as an external cavity and provide instantaneous linewidth narrowing (top middle), and the large mode volume Si_3N_4 coil resonator provides a stable frequency reference to lock the laser to (top right).

RESULTS

Hybrid integrated external cavity tunable laser (ECTL). The hybrid-integrated ECTL design, shown in Fig. 1, consists of a tunable silicon nitride external cavity made of two actuatable high-Q intra-cavity ring resonators, an adjustable phase section, and a tunable Sagnac loop mirror. The laser is hybrid integrated with a butt-coupled InP RSOA. The two high-Q rings, connected in an add-drop configuration, increase the effective cavity length of the laser and therefore the intra-cavity photon lifetime to provide instantaneous linewidth reduction. Thermo-optically tuned actuators on the ring resonators enable wide single mode tuning utilizing the Vernier effect, and the tunable Sagnac loop mirror serves as a broadband cavity reflector. The laser output is coupled to a lensed fiber. For hybrid integration, we edge couple a Thorlabs Single Angled Facet (SAF) C-band reflective SOA (1128C) to an 18 μm -wide, angled Si_3N_4 waveguide. The input waveguide is designed to optimize the modal overlap between the gain chip and the Si_3N_4 PIC before tapering down to 2.6 μm wide to achieve ultra-low propagation loss in the external cavity circuit (see Methods). The thermo-optically controlled ring resonators, with radii of 1998.36 and 2002.58 μm , have an FSR of ~ 126.5 pm and therefore a Vernier FSR of approximately 59.9 nm. The rings have an intrinsic-Q of 3.5 million (see Supplemental Note 2) and are designed to be over-coupled to reduce the lasing threshold, resulting in a loaded-Q of 0.65 million.

The measured ECTL performance is summarized in Figure 2. We demonstrate a 60 nm-wide single-mode operating range, from 1518.5 to 1578 nm (Fig. 2a), with a heater tuning efficiency of 54.5 nm/W (Fig. 2b) per actuator. We measure a side-mode suppression ratio (SMSR) of 65 dB (Fig. 2c) across the tuning range and a lasing threshold current of 63 mA (Fig. 2d). Fiber-coupled output power from the ECTL ranges from 0.23 mW at 1520 nm to 4.37 mW at 1578 nm. The change in output power is primarily due to the wavelength dependence of the Sagnac loop mirror. The frequency noise (FN) spectrum of the free-running widely tunable ECTL (without coil-resonator stabilization) is plotted for operation at 1550 nm in Fig. 2e, indicating the fundamental and integral linewidths of the free-running laser at this wavelength. The FN closely follows the calculated TRN limit of the ECTL rings (red-dashed) at > 100 kHz offset and reaches the white frequency noise (WFN) floor characteristic of the Lorentzian fundamental linewidth (FLW) at > 1 MHz frequency offset (the periodic high frequency spikes are from the Mach-Zehnder interferometer frequency noise measurement system). The WFN floor at 1550 nm is measured to be 1.93 Hz^2/Hz , corresponding to a 6.08 Hz (blue-dashed) FLW. The $1/\pi$ integral linewidth (ILW) of the free-running laser (without coil stabilization), at this wavelength, is calculated using the $1/\pi$ reverse integration method³⁰ to be 1.75 kHz and shown in the purple shaded region under the FN curve. Across the full tuning range, we measure the fundamental linewidth of the free-running ECTL to be in the range of 3 – 7 Hz as summarized in Fig. 2f (see Supplemental Note 4 for the full dataset).

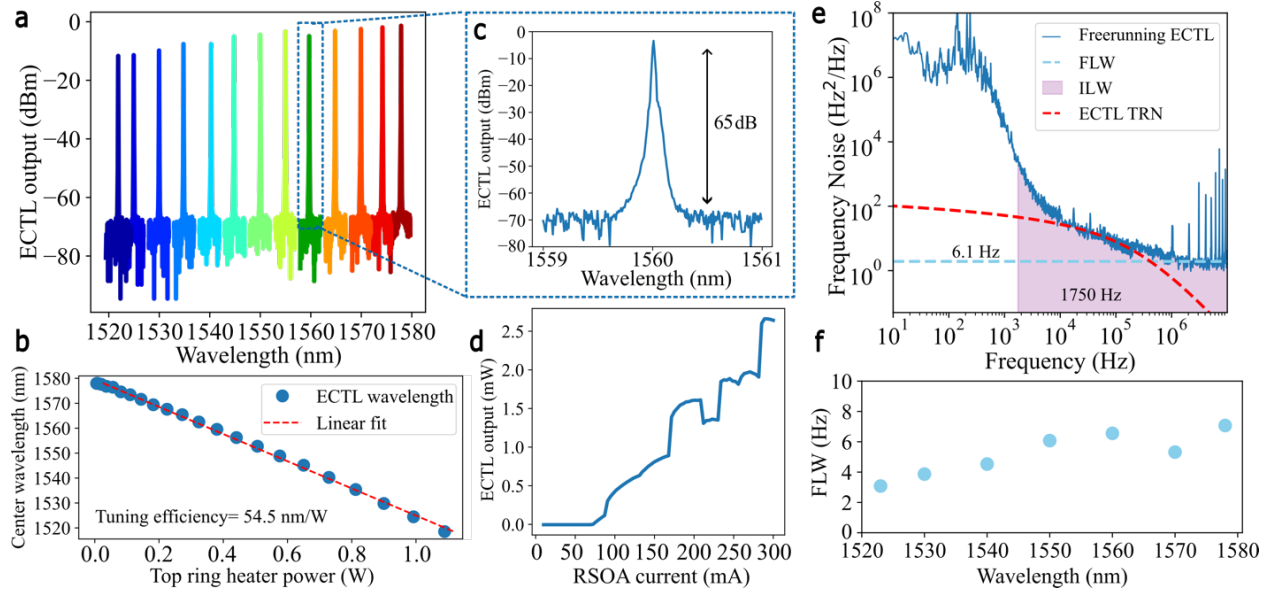


Fig. 2 External cavity tunable laser performance. **a** Single mode laser output from 1520 – 1580 nm. **b** Thermo-optic tuning of the top ring of the ECTL. **c** ECTL operation at 1560 nm with a measured SMSR of ~ 65 dB, measured on an OSA with RBW < 0.01 nm. **d** Fiber-coupled ECTL output power at 1550 nm vs. gain chip current, indicating a laser threshold current of 63 mA. The discontinuities are due to mode-hopping as the gain chip power increases, responding to slight changes in the coupling and temperature conditions of the PIC. **e** Frequency noise spectrum of the free-running ECTL at 1550 nm (blue, solid) measured using a fiber-MZI as an optical frequency discriminator. The blue dashed line plots the measured ECTL fundamental linewidth of 6.1 Hz, and the shaded purple region shows the area under the curve that contributes to the $1/\pi$ -integral linewidth of 1750 Hz. The red dashed curve plots a simulated estimate of the thermorefractive noise (TRN) limit of the ECTL rings. The high frequency spurs at multiples of 1 MHz correspond to the free-spectral range of the OFD fiber-MZI and do not contribute to the integral linewidth calculation. **f** Fundamental linewidth (FLW) of the ECTL measured across the 60 nm tuning range.

ECTL stabilization to an integrated SiN coil reference cavity. We stabilize the ECTL to a 10-meter-long silicon nitride integrated coil reference cavity without an optical isolator between the laser and reference cavity. Stabilization is achieved using a Pound-Drever-Hall (PDH) lock, as shown in Fig. 3. The 10-meter coil has a propagation loss of 0.2 dB/m and an intrinsic-Q of approximately 200 million. In addition to the low TRN limit, due to the large mode volume of the 10-meter cavity (see Fig. 4a red dashed curve), an important characteristic of the long coil resonator cavity is the small 20 MHz FSR. This aspect of the long coil-resonator ensures that there are resonances readily available to stabilize to for almost all operating wavelengths. See Supplemental Note 3 for more information on the 10-meter coil. As shown in Fig. 3 we use an electro-optic modulator (EOM) to generate sidebands and the PDH error signal is fed back directly to the ECTL gain chip current using a Vescent D2-125 laser servo. The ECTL takes on the FN characteristics of the coil resonator for frequency offsets up to the PDH locking bandwidth. Notably, the high internal quality factor of the ECTL, due to the low-loss ring resonators, provides high resilience to optical feedback and removes the need for an isolator to operate the stabilization lock circuit between the laser and the coil reference cavity. The elimination of the need for an optical isolator between the chips is important for future integration of the laser and coil reference

cavity onto a single silicon nitride chip. Hybrid integration of the gain chip allows realization of silicon nitride based laser cavities with large internal Q-factors that are inherently isolated and can withstand optical feedback without affecting the optical frequency noise characteristics; see refs ^{43,49,50} and Methods for more details. In future integrated versions, the EOM can be eliminated by using alternative approaches including directly tuning the laser frequency with PZT or thermal actuators, using PZT double sideband modulators, or employing modulation free stabilization techniques⁵³. Thermal and PZT actuators have been demonstrated in the SiN₃O₄ platform^{51,52}.

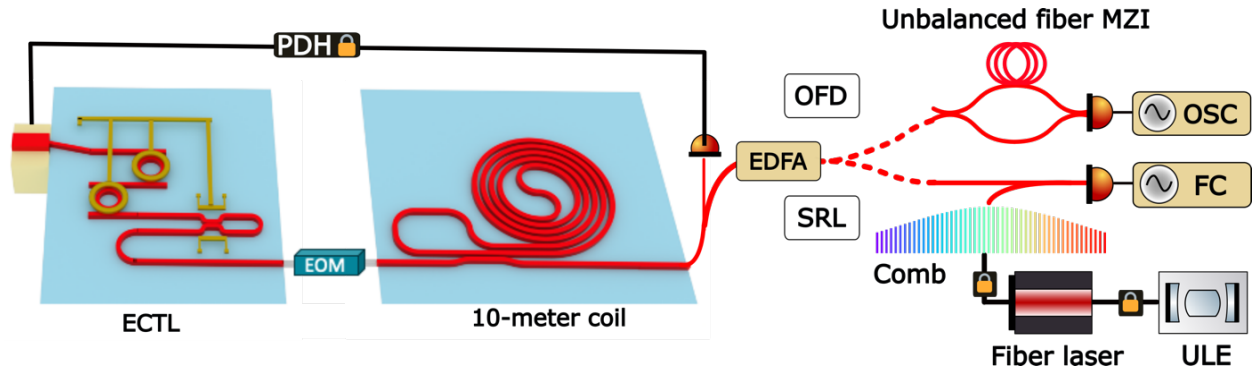


Fig. 3 Experimental setup of the integrated ECTL stabilized to an integrated coil reference cavity. a Schematic of the experimental setup where the ECTL is PDH-locked to an integrated 10-m coil reference cavity without an optical isolator. The frequency noise (FN) of the free-running and coil-locked ECTL is measured using two independent techniques: for FN below 3 kHz the ECTL output is mixed with a stable reference laser (SRL) that consists of an optical frequency comb locked to a single frequency Rock fiber laser that in turn is stabilized to an ultralow expansion (ULE) reference cavity, and the heterodyne beatnote signal is measured on a frequency counter (FC). For FN above 3 kHz an unbalanced fiber-MZI is used as an optical frequency discriminator (OFD) and the self-delayed homodyne signal is measured on a balanced photodiode and an oscilloscope (OSC).

The stabilized-ECTL frequency noise, linewidth, and Allan Deviation (ADEV) are measured using two independent techniques, outlined in Fig. 3. For FN above 3 kHz frequency offset we use an asymmetric fiber Mach-Zehnder interferometer (MZI) optical frequency discriminator (OFD). Below 3 kHz offset down to 1 Hz we measure the noise of a heterodyne beatnote of the ECTL with an optical frequency comb that has been locked to a stable reference laser (SRL). The beatnote is then measured on a precision frequency counter. See Methods for more details.

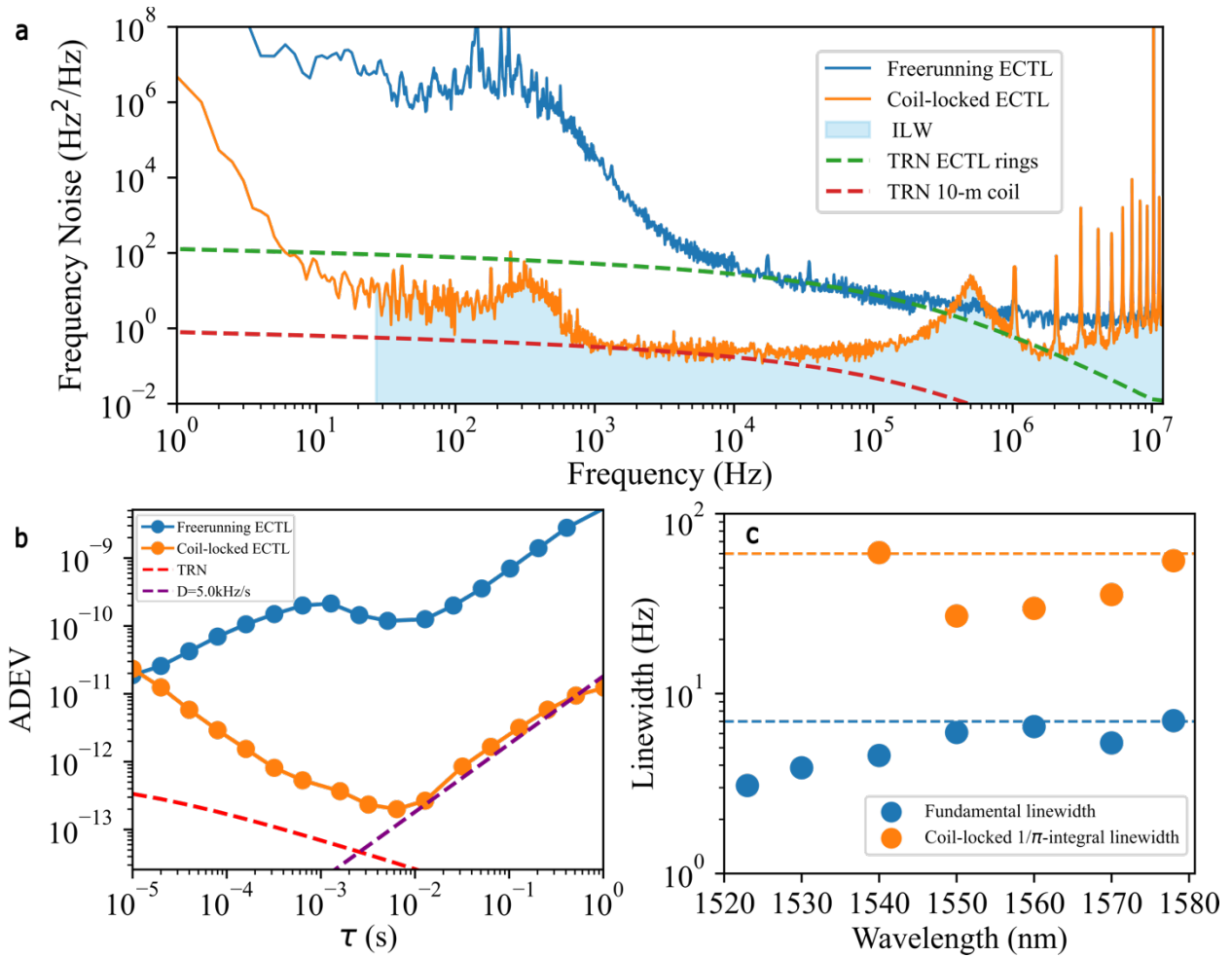


Fig. 4 Coil-stabilized ECTL frequency noise, stability, and fundamental and integral linewidths across tuning range. **a** An example frequency noise (FN) spectrum of the free-running (blue) and coil-locked (orange) ECTL at 1550 nm shows >5 orders of magnitude reduction in FN at low frequency offsets. The shaded light-blue area corresponds to the $1/\pi$ reverse integral linewidth (ILW) of the locked laser measured at 27 Hz. The minimum FN of the locked laser is measured at 0.12 Hz²/Hz at 16 kHz frequency offset. The PDH lock servo bump is indicated at 0.4 MHz. **c** Allan deviation (ADEV) of the free-running (blue) and coil-locked (orange) ECTL demonstrating 1.8×10^{-13} at 6.4 ms and 5 kHz/s drift. **d** The measured fundamental (blue) across the 60 nm tuning range and coil-locked integral (orange) linewidths across a 40 nm tuning range. The ILW measurement was limited by the beatnote measurement below 1540 nm. In addition, the coil-lock at 1520 nm and below was limited due to low extinction ratio (ER). The dashed lines indicate the highest measured value of 7 Hz for FLW (blue) and 60 Hz for ILW (orange).

The FN of the coil-locked ECTL operating at 1550 nm is plotted in Fig. 4a. The stabilized ECTL (orange) has a FN reduction of more than 5 orders of magnitude at low frequency offsets compared with the free-running laser (blue) and reaches the TRN limit of the 10-m coil resonator (red, dashed) between 1-100 kHz offset, before sloping upwards due to the servo bump corresponding to the PDH locking bandwidth at around 0.4 MHz. The measured $1/\pi$ integral linewidth of the stabilized-ECTL at 1550 nm is 27 Hz, reduced from 1750 Hz for the free-running laser, an integral linewidth reduction of 65x. The minimum FN is 0.12 Hz²/Hz at 16 kHz, and the corresponding fractional frequency stability, or Allan deviation (Fig. 4b), has a minimum of 1.8×10^{-13} at 6.4 ms

and a drift of 5 kHz/sec. The fundamental and integral linewidths of the stabilized-ECTL at various points across the tuning range are plotted in Fig. 4c, see Supplemental Note 4 for more details.

ECTL resilience to optical feedback. Optical feedback in a semiconductor laser can be quantified by the feedback parameter C ^{43,49,50},

$$C = \frac{\tau_{ext} r_{ext}}{\tau_{laser} r_{laser}} (1 - |r_{laser}|^2) \sqrt{1 + \alpha^2} \quad (1)$$

where r_{ext} and r_{laser} are the reflectivity of the external reflection and the laser mirror, τ_{ext} and τ_{laser} are the external cavity and laser cavity round trip lifetimes, and α is the linewidth enhancement factor. We compare the relative isolation of two lasers by taking the ratio of their C-parameters, $\frac{C_1}{C_2}$, since the ratio is only dependent on the attributes of the lasers and not on the specifics of the external reflection (i.e. not dependent on r_{ext} and τ_{ext}). The ECTL, compared with a conventional III-V DFB laser, has both a very high internal Q and high reflectivity, from which we estimate that $\frac{C_{ECTL}}{C_{DFB}} \sim 3.9 \times 10^4$, or approximately 45 dB (see Methods for more details). This therefore reduces or eliminates the need for an isolator for this stabilized laser result as well as for many applications.

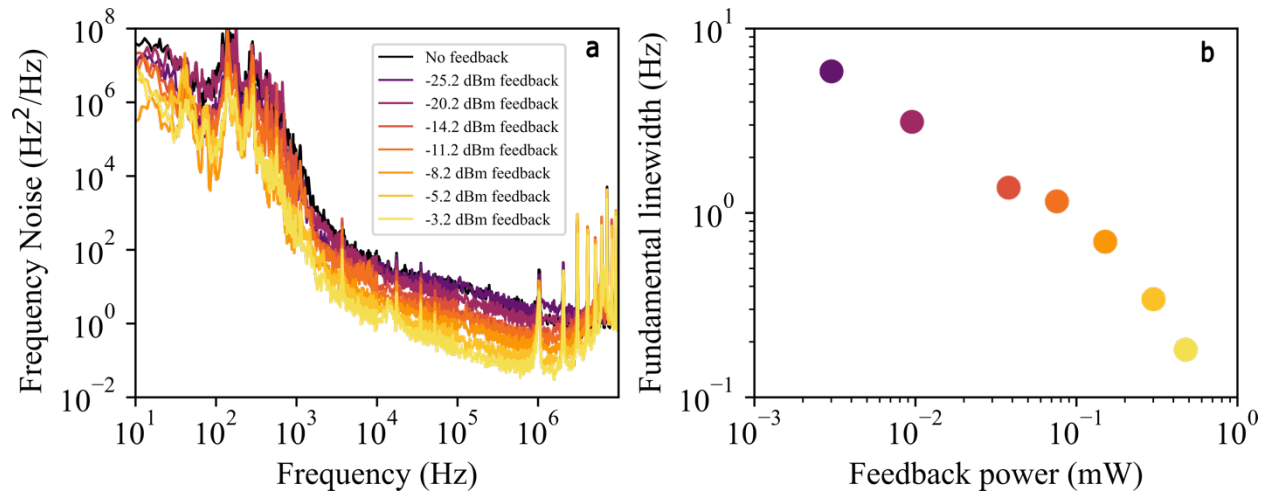


Fig. 5 ECTL feedback measurements. **a** Frequency noise plots of the free running ECTL operating at 1560 nm under different optical feedback levels ranging from -25 to -3 dBm. **b** Summary of frequency noise data from (a) in terms of the calculated fundamental linewidth (FLW) of the ECTL vs. the optical feedback power level, showing a decrease in FLW from 5.86 to 0.18 Hz with increased feedback.

This resilience to optical feedback is demonstrated by operating the PDH lock tying the ECTL to the 10-meter coil reference cavity without using an isolator: an important advantage for achieving a fully integrated stabilized laser on chip. To demonstrate this further and under controlled conditions with our ECTL we designed an optical feedback circuit (see Supplemental Note 5 for more details) where the ECTL output power is fed back to itself using a fiber circulator and a variable optical attenuator to control the optical feedback level. We then measure the OFD frequency noise of the ECTL under different feedback conditions, the results of which are plotted in Fig. 5. The ECTL remains single mode at all tested feedback levels, confirmed by the ability to

make OFD measurements and by monitoring on an OSA. We observe that the measured fundamental linewidth of the ECTL decreases with increasing optical feedback, at a rate inversely proportional to the feedback level. We believe there are two possible reasons for the linewidth narrowing. The first is related to the long coherence time and strong mode selectivity of the ECTL where the external feedback is coherent with photons stored in the laser leading to an increase in the intracavity number of photons which serves to drive down the fundamental linewidth. A second possible reason, as subject of future investigation, is the ECTL may be entering a self-injection locking regime.

DISCUSSION

In this paper we demonstrate a precision ultra-low instantaneous and integral linewidth stabilized widely tunable ECTL locked to an integrated coil reference cavity that achieves record-low frequency and phase noise for hybrid-integrated widely tunable lasers. The coil-locked ECTL realizes 6 Hz fundamental linewidth with 27 Hz integral linewidth and 1.8×10^{-13} fractional frequency stability at 1550 nm, and 3 - 7 Hz fundamental with sub-60 Hz integral linewidths measured across the tuning range. These fundamental linewidths are the lowest to date over the widest tuning range and the coil resonator stabilized integral linewidths are the lowest for integrated chips and across a wide tuning range reported to date. Furthermore, we demonstrate isolation free stabilization of the ECTL to the coil cavity, enabled by the high Q of the ECTL cavity. The 10-meter coil has an FSR of 20 MHz which allows locking and stabilization at almost all wavelengths across the tuning range, a distinct advantage from low FSR bulk optic reference cavities.

We compare our results to the state of the art in Table 1 and Fig. 6 with other hybrid-integrated low noise lasers. The table is sparsely populated in several columns since this work represents one of the few that report the $1/\pi$ integral linewidth which is important for many precision applications. When not available directly in the publication we have calculated the ILW from the available FN data in that publication. We believe this comparison highlights the unique properties of the hybrid-integrated ECTL locked to the integrated coil reference cavity. For example, we report both the fundamental and integral linewidths over a full tuning range of 60 nm. The fundamental linewidth is almost 1.5X lower and the $1/\pi$ integral linewidth 3 orders of magnitude lower than that reported in [45] and the tuning range is 1.5X larger than the laser reported in [45]. To date, this work is the first to report stabilization (ADEV) and isolator free operation (isolation of 45 dB).

Table 1. Comparison of low linewidth hybrid-integrated tunable lasers

Platform	Laser type	λ (nm)	FLW (Hz)	ILW (Hz) $1/\pi$	ADEV (@ 1 ms)	Tuning (nm)	Output power (mW)	SMSR (dB)	Optical isolation (dB)
Si ₃ N ₄ ⁵⁴	SIL	1550	0.04	236*	...	0.8	0.3	60	...
Si ₃ N ₄ ⁴¹	SIL	1550	3.8	4,715*	10.5	65	...
Si ₃ N ₄ ⁵⁵	SIL	1550	3	1,560*	54	...
Si ₃ N ₄ ¹⁷	SIL	780	0.74	864	...	2	2	36	...
Si ₃ N ₄ ⁵⁶	SIL	785	700	50,173*	...	12	10	37	...
Si ₃ N ₄ ²³	EDBR	1550	320	47,466*	24	55	...
Si ⁵⁷	ECTL: 3 ring	1550	220	33,246*	...	110	3	50	...
Si ⁵⁸	ECTL: 3 ring	1550	95	9,237*	...	120	1.5	60	...
Si ₃ N ₄ ³⁸	ECTL: 3 ring	1550	40	87,844**	...	70	23	60	...
Si ₃ N ₄ ⁵⁹	ECTL: 2 ring	1550	2,200	57,526*	...	120	24	63	...
Si ₃ N ₄ ⁴⁴	ECTL: 2 ring	1550	750 - 4,000	31,614*	...	172	26	68	...
Si ₃ N ₄ ⁴⁸	ECTL: 2 ring	852	65	6,770*	...	15	25	50	...
Si ₃ N ₄ ⁴⁵	ECTL: 2 ring	1550	6 - 9.8***	2,350	...	40	4.8	64	...
Si₃N₄[†]	ECTL (2 ring) + coil	1550	3 - 7***	27	1.8E-13 @ 6.4 ms	60	4.4	65	-45

† This work

* Not reported in manuscript: calculated from published FN data

** ILW limited by available FN data

*** Measured across tuning range

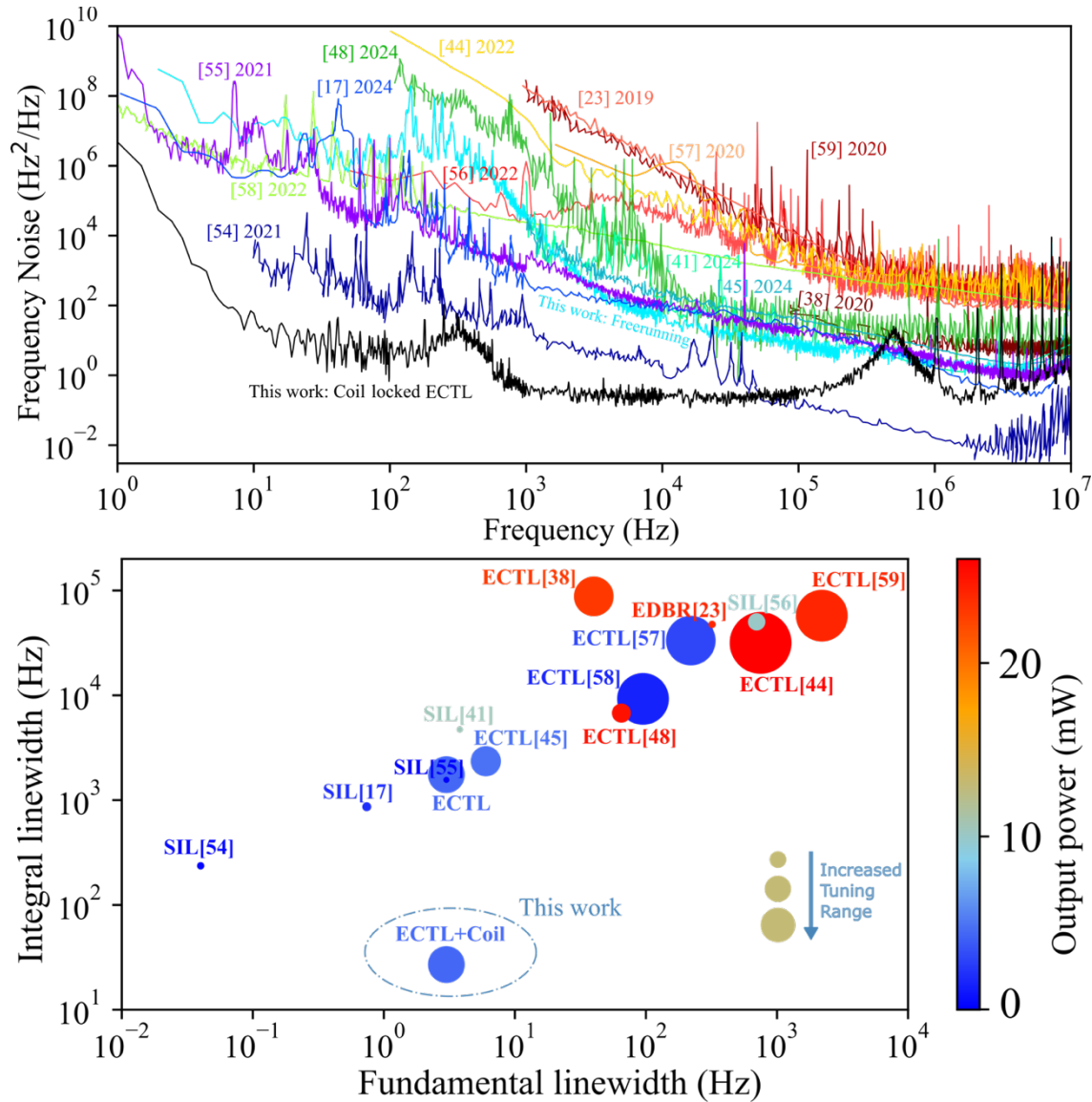


Fig. 6 Comparison of low linewidth hybrid-integrated lasers summarized in Table 1. a Frequency noise plots comparing hybrid-integrated low noise lasers. **b** Fundamental vs. $1/\pi$ integral linewidths. The bubble size represents the tuning range and color heat map represents output power.

Since both the ECTL and coil resonator are designed and fabricated in the same 80 nm thick, CMOS-compatible Si_3N_4 platform these results present a clear path forward towards realizing a fully integrated, chip-scale stabilized laser that combines narrow instantaneous linewidth with low frequency drift in one device. To achieve such a device, the EOM used in this experiments can be replaced by a PZT-on- Si_3N_4 piezo-optic modulator for locking bandwidths up to 20 MHz with low power consumption and that has already been demonstrated in the same platform³³. Alternatively, an all-optical, modulation-free design for generating a PDH error signal has also been demonstrated⁶⁰ and could be leveraged in future designs⁵³. Additionally, the core components of this stabilized laser design, namely the high-Q ring resonators and coil reference cavity, have already been demonstrated in this Si_3N_4 platform across the visible to near-IR (NIR) range^{20,36}

making this hybrid-integrated stabilized laser design a viable option for applications that require narrow linewidth stable lasers at visible and NIR wavelengths such as atomic and quantum applications. Chip-scale stabilized sources, in combination with photonic integrated beam delivery, are necessary to reduce the size, complexity and cost of several key quantum technologies such as compact cold atom⁶¹ and trapped ion^{36,62} systems.

Further experiments and design improvements will yield better laser performance in terms of tunability, variation in integral and fundamental linewidth, and higher output power. For example, full control of the Sagnac loop mirror would provide an adjustment of the laser output power, and therefore also the intracavity power, allowing the user to optimize for higher output power versus lower fundamental linewidth. Additionally, loaded-Qs as high as 100 million have been demonstrated in this platform⁶³, and since the modified Schawlow-Townes laser linewidth will decrease as $1/Q^2$, we predict that future devices could achieve even lower fundamental linewidths. Future designs can also include coil resonators longer than 10-meters to increase the mode volume and further reduce the TRN and integral linewidth, as well as incorporating tunable coupling⁶³ to optimize the laser locking conditions across a wide range of wavelengths using a single resonator. For applications that require high optical output power additional gain blocks can be added and operated in parallel with a shared high-Q silicon nitride external cavity⁶⁴ where output powers >100 mW have already been demonstrated in a dual-gain hybrid-integrated laser⁴⁶. Other pathways to increasing the output power are to incorporate on-chip amplifiers^{65,66} or through injection-locked amplification.

METHODS

Fabrication process. The lower cladding consists of a 15- μm -thick thermal oxide grown on a 100 mm diameter, 1 mm thick silicon wafer substrate. The main waveguide layer is an 80 nm thick stoichiometric Si_3N_4 film deposited on the lower cladding using low-pressure chemical vapor deposition (LPCVD). A PAS 5500 ASML deep ultraviolet (DUV) stepper was used to pattern a DUV photoresist layer. The high-aspect-ratio waveguide core is formed by anisotropically dry etching the Si_3N_4 film in a Panasonic E626I Inductively Coupled Plasma-Reactive Ion etcher (ICP-RIE) using a $\text{CHF}_3/\text{CF}_4/\text{O}_2$ chemistry. After the etch, the wafer is cleaned using a standard RCA cleaning process. A 5- μm -thick silicon dioxide upper cladding layer was deposited using plasma-enhanced chemical vapor deposition (PECVD) with tetraethoxysilane (TEOS) as a precursor. This is followed by a final two-step anneal at 1050 °C for 7 hours and 1150 °C for 2 hours which is an optimized anneal process for our waveguides.

RSOA coupling. The gain chip is coated with 90% reflectivity on the side opposite the silicon nitride PIC and an antireflection (AR) material on the near side with a reflectivity of 0.005%. It is then mounted on a temperature-controlled copper block for heat-sinking. The gain chip is wire bonded to a PCB that screws onto the copper block for external electrical control of the gain chip. The SOA has an angled facet of 5.6 degrees that requires, based on Snell's Law, the Si_3N_4

waveguide to be angled by 13.1 degrees to best match the beam propagation direction. The Si₃N₄ waveguide is initially 18 μm-wide to achieve an estimated optimal mode overlap of 52%. We estimate that the actual coupling loss is around 4-5 dB. The Si₃N₄ PIC sits atop its own temperature-controlled mount and the RSOA is edge-coupled to the ECTL input waveguide.

Frequency noise measurements. The ECTL frequency noise, linewidth, and stability is measured using two independent techniques^{20,21,30,67,68}. For FN above 3 kHz frequency offset we use an unbalanced fiber-MZI with a 1.026 MHz FSR as an optical frequency discriminator (OFD) and measure the self-delayed homodyne FN signal on a high-speed balanced photodetector. Below 3 kHz offset the OFD fiber-MZI noise can become dominant so we instead photomix the ECTL with a stable reference laser (SRL) and measure the heterodyne beatnote signal with a Keysight 53230A precision frequency counter. The SRL system consists of a single frequency Rock fiber laser PDH-locked to a Stable Laser Systems (SLS) 1550 nm ultralow expansion (ULE) cavity that delivers Hz-level linewidth and ~0.1 Hz/s frequency drift. Additionally, we use a Vescent self-referenced fiber frequency comb with a 100 MHz f_{rep} and lock it to the SLS to extend the stability of the SRL system to many wavelengths and enable accurate close-to-carrier FN measurements across the ECTL spectrum.

Optical isolation measurement. In equation (1) we introduced the optical feedback parameter C that was first defined by Petermann⁶⁹ to describe feedback in a semiconductor laser. We can then compare the relative isolation of two lasers by taking the ratio of their C -parameters where the ratio is only dependent on characteristics of the laser: τ , r and α .

$$\frac{C_1}{C_2} = \frac{\tau_{\text{laser}_2} r_{\text{laser}_2} \frac{1-|r_{\text{laser}_1}|^2}{1-|r_{\text{laser}_2}|^2} \sqrt{1+\alpha_1^2}}{\tau_{\text{laser}_1} r_{\text{laser}_1} \frac{1-|r_{\text{laser}_2}|^2}{1-|r_{\text{laser}_1}|^2} \sqrt{1+\alpha_2^2}} \quad (2)$$

The robustness of our ECTL to feedback light arises predominantly from two attributes. The first, is the extended cavity photon lifetime, τ_{laser} , due to the two high-Q intracavity rings. We can approximate the overall roundtrip photon lifetime of the dual-ring ECTL as a sum of the Fabry-Perot (FP) and individual ring resonator cavity lifetimes⁷⁰. The FP cavity is formed by the back mirror of the RSOA (R_1) and the Si₃N₄ waveguide Sagnac loop mirror (R_2), and subject to internal losses (η), such as the coupling loss at the interface between the gain chip and the PIC, and has an associated lifetime of:

$$\tau_{\text{FP}} = \frac{-2L}{c} \ln(R_1 R_2 (1 - \eta)^2)^{-1} \quad (3)$$

The rings each contribute an additional $\tau_{\text{RR}} = \frac{\lambda Q}{2\pi c}$ and one full roundtrip requires four passes through a ring: $\tau_{\text{ectl}} = \tau_{\text{FP}} + 4\tau_{\text{RR}}$. For the ECTL we estimate that $\tau_{\text{ectl}} = 2.3$ ns. The second attribute that contributes to the robustness to optical feedback is the relatively high reflectivity of the Sagnac loop mirror, which for our design is ~75%. The low loss intracavity rings store enough power within the cavity to support a high mirror reflectivity and still provide useful output power from the laser. Compared to a conventional III-V DFB laser that has an internal Q of $\sim 1 \times 10^4$ and

front mirror reflectivity of $<1\%$, we estimate from equation (2) that the ECTL has inherent isolation of approximately 45 dB.

DATA AVAILABILITY

The data that support the plots within this paper and other findings of this study are available from the corresponding author on reasonable request.

REFERENCES

1. Ludlow, A. D., Boyd, M. M., Ye, J., Peik, E. & Schmidt, P. O. Optical atomic clocks. *Rev. Mod. Phys.* **87**, 637–701 (2015).
2. Norcia, M. A. *et al.* Seconds-scale coherence on an optical clock transition in a tweezer array. *Science* **366**, 93–97 (2019).
3. Loh, W. *et al.* Optical Atomic Clock Interrogation Via an Integrated Spiral Cavity Laser. Preprint at <http://arxiv.org/abs/2403.12794> (2024).
4. Bruzewicz, C. D., Chiaverini, J., McConnell, R. & Sage, J. M. Trapped-ion quantum computing: Progress and challenges. *Applied Physics Reviews* **6**, 021314 (2019).
5. Ladd, T. D. *et al.* Quantum computers. *Nature* **464**, 45–53 (2010).
6. Abramovici, A. *et al.* LIGO: The Laser Interferometer Gravitational-Wave Observatory. *Science* **256**, 325–333 (1992).
7. Degen, C. L., Reinhard, F. & Cappellaro, P. Quantum sensing. *Rev. Mod. Phys.* **89**, 035002 (2017).
8. Fan, H. *et al.* Atom based RF electric field sensing. *J. Phys. B: At. Mol. Opt. Phys.* **48**, 202001 (2015).
9. Stray, B. *et al.* Quantum sensing for gravity cartography. *Nature* **602**, 590–594 (2022).
10. Marra, G. *et al.* Ultrastable laser interferometry for earthquake detection with terrestrial and submarine cables. *Science* **361**, 486–490 (2018).
11. Lindsey, N. J., Dawe, T. C. & Ajo-Franklin, J. B. Illuminating seafloor faults and ocean dynamics with dark fiber distributed acoustic sensing. *Science* **366**, 1103–1107 (2019).

12. Sun, S. *et al.* Integrated optical frequency division for microwave and mmWave generation. *Nature* **627**, 540–545 (2024).
13. Kudelin, I. *et al.* Photonic chip-based low-noise microwave oscillator. *Nature* **627**, 534–539 (2024).
14. Matei, D. G. *et al.* $1.5\ \mu\text{m}$ Lasers with Sub-10 mHz Linewidth. *Phys. Rev. Lett.* **118**, 263202 (2017).
15. Hirata, S., Akatsuka, T., Ohtake, Y. & Morinaga, A. Sub-hertz-linewidth diode laser stabilized to an ultralow-drift high-finesse optical cavity. *Appl. Phys. Express* **7**, 022705 (2014).
16. Bishop, A. M. & Gaeta, A. L. Narrow linewidth semiconductor lasers based on nonlinear self-injection locking. Preprint at <https://doi.org/10.48550/arXiv.2309.09811> (2023).
17. Isichenko, A. *et al.* Sub-Hz fundamental, sub-kHz integral linewidth self-injection locked 780 nm hybrid integrated laser. *Sci Rep* **14**, 27015 (2024).
18. Kondratiev, N. M. *et al.* Recent advances in laser self-injection locking to high-Q microresonators. *Front. Phys.* **18**, 21305 (2023).
19. Li, B. *et al.* High-coherence hybrid-integrated 780-nm source by self-injection-locked second-harmonic generation in a high-Q silicon-nitride resonator. *Optica*, *OPTICA* **10**, 1241–1244 (2023).
20. Chauhan, N. *et al.* Visible light photonic integrated Brillouin laser. *Nat Commun* **12**, 4685 (2021).
21. Gundavarapu, S. *et al.* Sub-hertz fundamental linewidth photonic integrated Brillouin laser. *Nature Photon* **13**, 60–67 (2019).
22. Li, J., Lee, H., Chen, T. & Vahala, K. J. Characterization of a high coherence, Brillouin microcavity laser on silicon. *Opt. Express*, *OE* **20**, 20170–20180 (2012).
23. Xiang, C., Morton, P. A. & Bowers, J. E. Ultra-narrow linewidth laser based on a semiconductor gain chip and extended Si_3N_4 Bragg grating. *Opt. Lett.*, *OL* **44**, 3825–3828 (2019).
24. Santis, C. T., Steger, S. T., Vilenchik, Y., Vasilyev, A. & Yariv, A. High-coherence semiconductor lasers based on integral high- Q resonators in hybrid Si/III-V platforms. *Proc. Natl. Acad. Sci. U.S.A.* **111**, 2879–2884 (2014).

25. Tran, M. A., Huang, D. & Bowers, J. E. Tutorial on narrow linewidth tunable semiconductor lasers using Si/III-V heterogeneous integration. *APL Photonics* **4**, 111101 (2019).
26. Blumenthal, D. J., Heideman, R., Geuzebroek, D., Leinse, A. & Roeloffzen, C. Silicon Nitride in Silicon Photonics. *Proceedings of the IEEE* **106**, 2209–2231 (2018).
27. Puckett, M. W. *et al.* 422 Million intrinsic quality factor planar integrated all-waveguide resonator with sub-MHz linewidth. *Nat Commun* **12**, 934 (2021).
28. Liu, K. *et al.* Ultralow 0.034 dB/m loss wafer-scale integrated photonics realizing 720 million Q and 380 μ W threshold Brillouin lasing. *Opt. Lett.* **47**, 1855 (2022).
29. Chauhan, N. *et al.* Integrated 3.0 meter coil resonator for $\lambda = 674$ nm laser stabilization. in *Frontiers in Optics + Laser Science 2022 (FIO, LS) (2022), paper FM1E.1* FM1E.1 (Optica Publishing Group, 2022). doi:10.1364/FIO.2022.FM1E.1.
30. Liu, K. *et al.* 36 Hz integral linewidth laser based on a photonic integrated 4.0 m coil resonator. *Optica* **9**, 770 (2022).
31. Dong, M. *et al.* Piezo-optomechanical cantilever modulators for VLSI visible photonics. *APL Photonics* **7**, 051304 (2022).
32. Wen, Y. H. *et al.* High-speed photonic crystal modulator with non-volatile memory via structurally-engineered strain concentration in a piezo-MEMS platform. Preprint at <http://arxiv.org/abs/2310.07798> (2023).
33. Wang, J., Liu, K., Isichenko, A., Rudy, R. Q. & Blumenthal, D. J. Integrated programmable strongly coupled three-ring resonator photonic molecule with ultralow-power piezoelectric control. *Opt. Lett., OL* **48**, 2373–2376 (2023).
34. Bose, D. *et al.* Anneal-free ultra-low loss silicon nitride integrated photonics. *Light Sci Appl* **13**, 156 (2024).
35. He, Y. *et al.* Chip-scale high-performance photonic microwave oscillator. *Science Advances* **10**, eado9570 (2024).

36. Chauhan, N. *et al.* Trapped ion qubit and clock operations with a visible wavelength photonic coil resonator stabilized integrated Brillouin laser. Preprint at <http://arxiv.org/abs/2402.16742> (2024).
37. Chauhan, N. *et al.* Ultra-low loss visible light waveguides for integrated atomic, molecular, and quantum photonics. *Opt. Express, OE* **30**, 6960–6969 (2022).
38. Fan, Y. *et al.* Hybrid integrated InP-Si₃N₄ diode laser with a 40-Hz intrinsic linewidth. *Opt. Express, OE* **28**, 21713–21728 (2020).
39. Lihachev, G. *et al.* Frequency agile photonic integrated external cavity laser. Preprint at <http://arxiv.org/abs/2303.00425> (2023).
40. Lihachev, G. *et al.* Ultralow-noise frequency-agile photonic integrated lasers. Preprint at <http://arxiv.org/abs/2104.02990> (2021).
41. Siddharth, A. *et al.* Piezoelectrically tunable, narrow linewidth photonic integrated extended-DBR lasers. *Optica, OPTICA* **11**, 1062–1069 (2024).
42. Huang, G. *et al.* Thermorefractive noise in silicon-nitride microresonators. *Phys. Rev. A* **99**, 061801 (2019).
43. Harfouche, M. *et al.* Kicking the habit/semiconductor lasers without isolators. *Opt. Express* **28**, 36466 (2020).
44. Guo, Y. *et al.* Hybrid integrated external cavity laser with a 172-nm tuning range. *APL Photonics* **7**, 066101 (2022).
45. Wu, Y. *et al.* Hybrid integrated tunable external cavity laser with sub-10 Hz intrinsic linewidth. *APL Photonics* **9**, 021302 (2024).
46. Boller, K.-J. *et al.* Hybrid Integrated Semiconductor Lasers with Silicon Nitride Feedback Circuits. *Photonics* **7**, 4 (2020).
47. Franken, C. a. A. *et al.* Hybrid-integrated diode laser in the visible spectral range. *Opt. Lett., OL* **46**, 4904–4907 (2021).
48. Nejadriahi, H. *et al.* Sub-100 Hz Intrinsic Linewidth 852 nm Silicon Nitride External Cavity Laser. Preprint at <https://doi.org/10.48550/arXiv.2409.17382> (2024).

49. Zhang, Z. *et al.* High-Speed Coherent Optical Communication With Isolator-Free Heterogeneous Si/III-V Lasers. *Journal of Lightwave Technology* **38**, 6584–6590 (2020).
50. Gomez, S. *et al.* High coherence collapse of a hybrid III–V/Si semiconductor laser with a large quality factor. *J. Phys. Photonics* **2**, 025005 (2020).
51. Wang, J., Liu, K., Harrington, M. W., Rudy, R. Q. & Blumenthal, D. J. Silicon nitride stress-optic microresonator modulator for optical control applications. *Opt. Express, OE* **30**, 31816–31827 (2022).
52. Wang, J., Liu, K., Rudy, R. Q. & Blumenthal, D. J. AOM-Free Laser Stabilization using integrated Silicon Nitride Carrier-Tracking Stress-Optic Modulator and Reference Cavity. in *Optica Quantum 2.0 Conference and Exhibition (2023)*, paper QW3B.3 QW3B.3 (Optica Publishing Group, 2023). doi:10.1364/QUANTUM.2023.QW3B.3.
53. Liu, K., Harrington, M. W., Wang, J., Nelson, K. D. & Blumenthal, D. J. Integrated self-delayed 2-m coil-resonator for high sensitivity optical frequency discrimination and laser linewidth narrowing. in *Frontiers in Optics + Laser Science 2023 (FiO, LS) (2023)*, paper JW4A.22 JW4A.22 (Optica Publishing Group, 2023). doi:10.1364/FIO.2023.JW4A.22.
54. Li, B. *et al.* Reaching fiber-laser coherence in integrated photonics. *Opt. Lett., OL* **46**, 5201–5204 (2021).
55. Xiang, C. *et al.* High-performance lasers for fully integrated silicon nitride photonics. *Nat Commun* **12**, 6650 (2021).
56. Corato-Zanarella, M. *et al.* Widely tunable and narrow-linewidth chip-scale lasers from near-ultraviolet to near-infrared wavelengths. *Nat. Photon.* **17**, 157–164 (2023).
57. Tran, M. A. *et al.* Ring-Resonator Based Widely-Tunable Narrow-Linewidth Si/InP Integrated Lasers. *IEEE Journal of Selected Topics in Quantum Electronics* **26**, 1–14 (2020).
58. Morton, P. A. *et al.* Integrated Coherent Tunable Laser (ICTL) With Ultra-Wideband Wavelength Tuning and Sub-100 Hz Lorentzian Linewidth. *Journal of Lightwave Technology* **40**, 1802–1809 (2022).

59. Rees, A. van *et al.* Ring resonator enhanced mode-hop-free wavelength tuning of an integrated extended-cavity laser. *Opt. Express, OE* **28**, 5669–5683 (2020).
60. Idjadi, M. H., Kim, K. & Fontaine, N. K. Modulation-free laser stabilization technique using integrated cavity-coupled Mach-Zehnder interferometer. *Nat Commun* **15**, 1922 (2024).
61. Isichenko, A. *et al.* Photonic integrated beam delivery for a rubidium 3D magneto-optical trap. *Nat Commun* **14**, 3080 (2023).
62. Niffenegger, R. J. *et al.* Integrated multi-wavelength control of an ion qubit. *Nature* **586**, 538–542 (2020).
63. Liu, K. *et al.* Tunable broadband two-point-coupled ultra-high- Q visible and near-infrared photonic integrated resonators. *Photon. Res., PRJ* **12**, 1890–1898 (2024).
64. Zhao, R. *et al.* Hybrid dual-gain tunable integrated InP-Si₃N₄ external cavity laser. *Opt. Express* **29**, 10958 (2021).
65. Beeck, C. O. de *et al.* Heterogeneous III-V on silicon nitride amplifiers and lasers via microtransfer printing. *Optica, OPTICA* **7**, 386–393 (2020).
66. Mu, J., Dijkstra, M., Korterik, J., Offerhaus, H. & García-Blanco, S. M. High-gain waveguide amplifiers in Si₃N₄ technology via double-layer monolithic integration. *Photon. Res., PRJ* **8**, 1634–1641 (2020).
67. Liu, K. *et al.* Common cavity waveguide coil-resonator stabilized hybrid integrated WDM laser with 89 Hz integral linewidth. in *2024 Optical Fiber Communications Conference and Exhibition (OFC)* 1–3 (2024).
68. Liu, K. *et al.* Photonic circuits for laser stabilization with integrated ultra-high Q and Brillouin laser resonators. *APL Photonics* **7**, 096104 (2022).
69. Petermann, K. External optical feedback phenomena in semiconductor lasers. *IEEE Journal of Selected Topics in Quantum Electronics* **1**, 480–489 (1995).
70. Oldenbeuving, R. M. *et al.* 25 kHz narrow spectral bandwidth of a wavelength tunable diode laser with a short waveguide-based external cavity. *Laser Phys. Lett.* **10**, 015804 (2012).

ACKNOWLEDGEMENT

We acknowledge Henry Timmers at Vescent for help with the setup of the fiber frequency comb and Mark W. Harrington at UCSB for help with the SRL system. This work is based in part by funding from the DARPA GRYPHON contract HR0011-22-2-0008. The views and conclusions contained in this document are those of the author(s) and should not be interpreted as representing the official policies of DARPA or the U.S. government.

AUTHOR CONTRIBUTIONS

DASH, DJB, DB, KL and AI prepared the manuscript. DB designed and fabricated the ECTL PICs. DASH built the laser with help from AI. DASH characterized the ECTL performance. KL designed and tested the coil resonator which was fabricated by Karl Nelson. DASH and KL performed all laser locking and frequency noise experiments. AI built the SRL and optical frequency comb frequency noise measurement system. DJB supervised the project.

COMPETING INTERESTS

Dr. Blumenthal's work has been funded by ColdQuanta d.b.a. Inflection. Dr. Blumenthal has consulted for Inflection and received compensation, is a member of the scientific advisory council, and owns stock in the company. D. A. S. Heim, D. Bose, K. Liu, and A Isichenko, declare no potential conflict of interest.

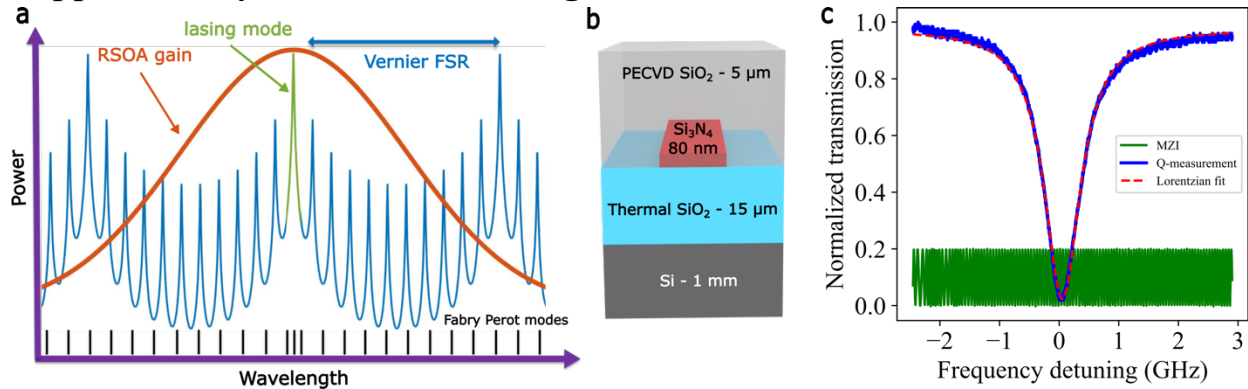
Supplemental information

Supplementary Note 1: Introduction

This supplemental section provides additional information on the design and performance of the hybrid-integrated external cavity tunable laser (ECTL), including a diagram of the working principle of the dual-ring ECTL, measurement of the ring resonator Qs, measurements of the 10-meter coil resonator, more information regarding the freerunning and integrated coil-stabilized frequency noise measurements, as well as a demonstration of the ECTL operating without an isolator under direct feedback.

The basic working principle of the dual-ring ECTL is illustrated in Supplementary Fig. 1a. The RSOA has a broad power spectrum and the two ring resonators, with slightly different radii, provide linewidth narrowing where the two resonances overlap. Changing the resonance of one of the rings adjusts which modes overlap and thereby tunes the laser up to one Vernier FSR. In addition to the ring resonances there are also Fabry Perot modes of the external cavity that bunch up near the lasing mode. It is necessary that the linewidth of the main lasing mode be narrower than the Fabry Perot cavity mode spacing.

Supplementary Note 2: ECTL design

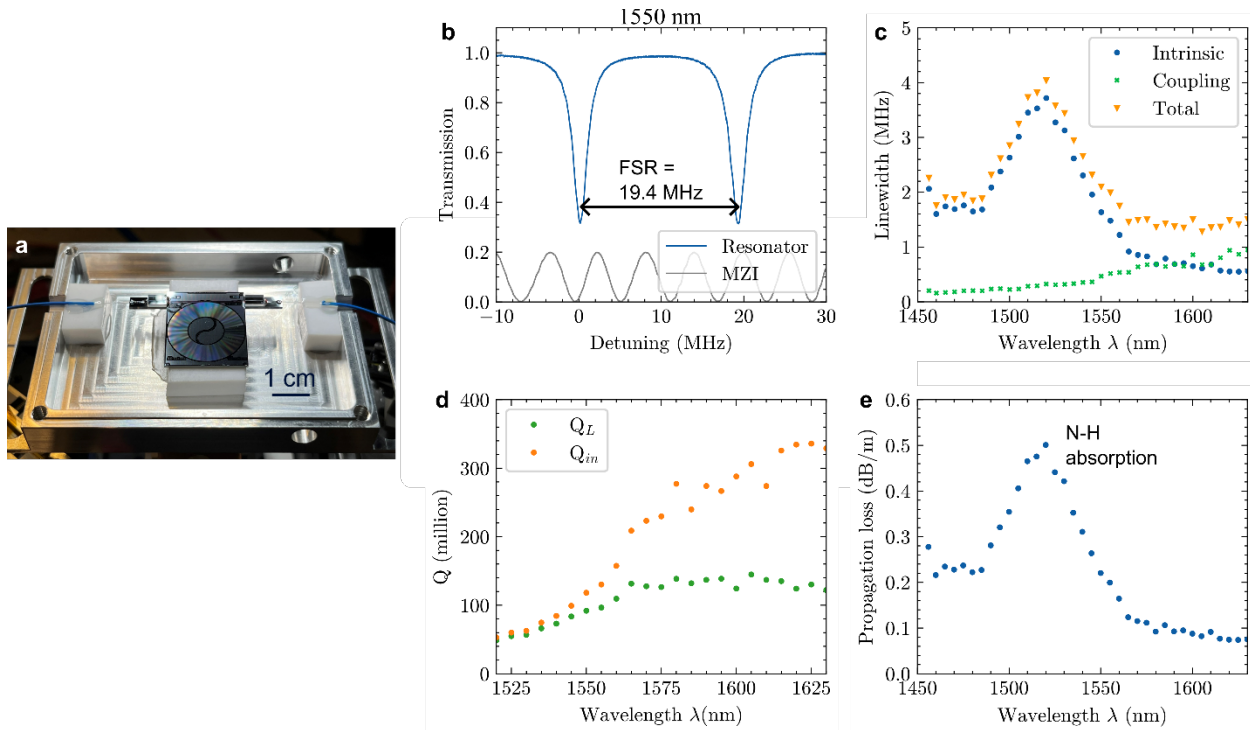


Supplementary Fig. 1 ECTL working principle and characterization. **a** An illustration of the basic working principle of the dual-ring external cavity tunable laser (ECTL). **b** The layer stack of both the ECTL and the 10-meter coil resonator. **c** Q-measurement of one of the ECTL rings (blue) fitted to a Lorentzian function (red) to extract Q values of 0.65 million loaded and 3.5 million intrinsic. An 18 MHz fiber-MZI (green) is used to calibrate the frequency detuning.

The layer stack for the low-loss Si_3N_4 waveguide platform is indicated in Supplementary Fig. 1b. The ECTL waveguide width is $2.6 \mu\text{m}$ resulting in a dilute optical mode to reduce scattering losses. Measurement of the quality factor (Q) of the intracavity rings, shown in Supplementary Fig. 1c, yield loaded and intrinsic-Qs of 0.6 and 3.5 million, respectively. The rings were intentionally heavily coupled to reduce cavity coupling losses to lower the lasing threshold at the expense of having higher loaded-Qs for the intra-cavity rings. This is a design parameter that can be optimized in future designs.

Supplementary Note 3: 10-meter-coil resonator design and characterization

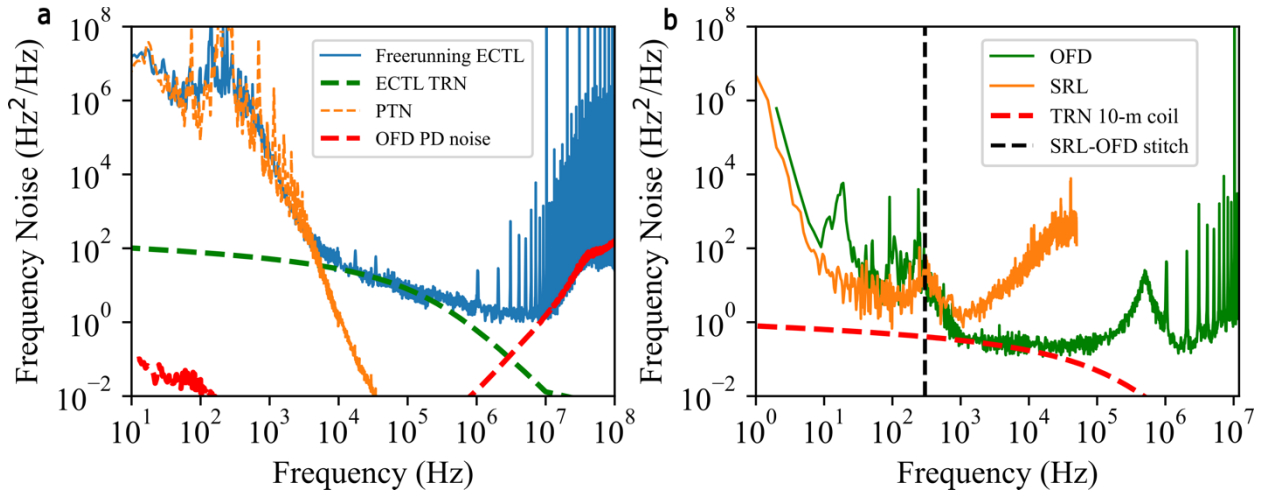
The coil resonator employs the same silicon nitride waveguide thickness of 80 nm as the ECTL laser chip, while the waveguide width is different. The waveguide design in the 10-meter-coil resonators has the waveguide dimension of $6 \mu\text{m}$ by 80 nm with the fundamental TE mode. The coil spiral center-to-center waveguide spacing is $25 \mu\text{m}$, and the circular S-bend diameter in the center of the coil waveguides is $\sim 3.6 \text{ mm}$, resulting in a much smaller device size and making it possible to wrap the 10-meter-coil waveguide on a single die size (21.6 mm by 26 mm). The bus-resonator directional coupler uses a $2.5 \mu\text{m}$ coupler gap and 1.5 mm coupling length. The bus waveguide is tapered from $6 \mu\text{m}$ to $1.5 \mu\text{m}$ for better fiber-to-chip edge coupling. The fiber-pigtailed device is packaged with a metal enclosure for better handling capabilities, shown in Supplementary Fig. 2a. The FSR is measured to be around 19.4 MHz, and the intrinsic Q reaches above 300 million around 1600 nm, shown in Supplementary Fig. 2d.



Supplementary Fig. 2. 10-meter-coil waveguide reference resonator design and testing. **a** 10-meter-coil resonator with PM-SMF28 fibers pig-tailed and packaged in a metal enclosure. **b** Spectral scan of the coil resonator resolves the resonance linewidth and FSR. **c** Intrinsic, coupling and total resonator linewidths in MHz are measured from 1450 nm to 1630 nm. **d** Intrinsic and loaded Qs are estimated from the resonator linewidth measurements. **e** Waveguide propagation loss is also estimated, showing an absorption peak around 1520 nm.

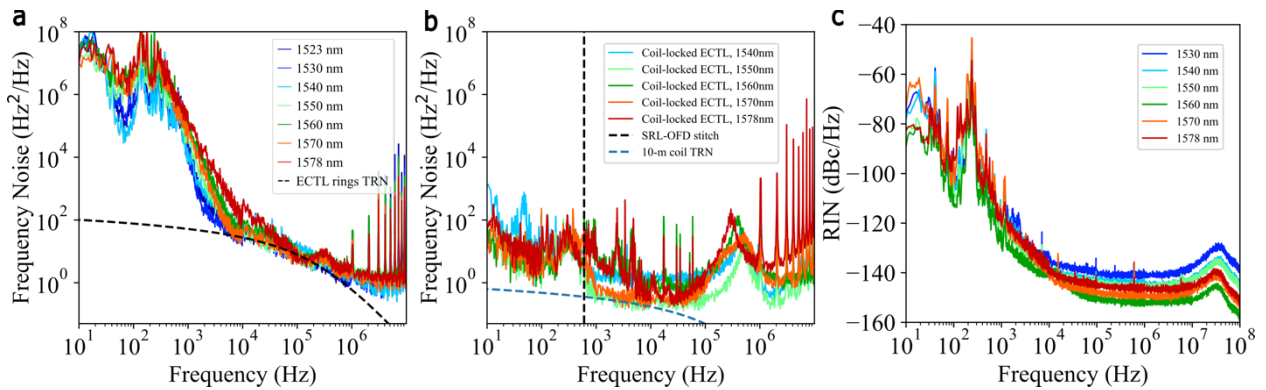
Supplementary Note 4: Frequency noise measurements

To measure the frequency noise (FN) of the free running and coil-stabilized ECTL we utilize two independent measurement techniques. Plotted in Supplementary Fig. 3a is the FN of the free running ECTL (blue) measured using an unbalanced fiber-MZI as an optical frequency discriminator (OFD) and reading out the self-delayed homodyne signal on a balanced photodiode. The dashed lines in red, green, and orange indicate calculated estimates of the noise floors of the photodetector noise, thermal refractive noise and photothermal noise of the ECTL intracavity ring resonators. When we stabilize the ECTL to the 10-meter coil reference cavity the FN at certain low frequency offsets drops by five orders of magnitude, in which case noise due to the fiber-MZI can dominate over the laser noise. To resolve this, we include additional close-to-carrier (CTC) measurements for the locked ECTL by mixing it with a stable reference laser (SRL) system and measuring the heterodyne beatnote signal on a frequency counter. The SRL system includes a Vescent fiber frequency comb locked to a single frequency Rock fiber laser that is itself locked to an ultralow expansion (ULE) cavity. The CTC measurement of the stabilized-ECTL is plotted in Supplementary Fig. 3b (orange) and becomes limited by the speed of the frequency counter at frequency offsets above ~ 1 kHz. The OFD measurement of the locked-ECTL is plotted (green), and the two can be stitched together (vertical black line) to give a more accurate measurement of the laser FN and to calculate the integral linewidth. See refs ¹⁻⁵ for more information.



Supplementary Fig. 3 ECTL frequency noise measurements. **a** Frequency noise (FN) power spectrum of the freerunning ECTL (blue) at 1550 nm measured using an MZI as an optical frequency discriminator. The orange, red, and green dashed curves are calculated estimates of the thermal refractive and photothermal noise floor of the two intracavity rings and the OFD photodetector noise, respectively. **b** FN of the coil-locked laser measured using two methods: OFD delayed self-homodyne (green) and Stable Reference Laser (SRL) heterodyne beatnote (orange). The black vertical lines indicates where the two are stitched together for the composite locked-ECTL measurements.

The ECTL operates across 60 nm tuning. FN measurements of the freerunning and locked ECTL across the tuning range are plotted in Supplementary Fig. 4a,b showing fundamental linewidths between 3-7 Hz and $1/\pi$ -integral linewidths from 27 to 60 Hz. Relative intensity noise (RIN) measurements across the ECTL tuning range are also included in Supplementary Fig. 4c.

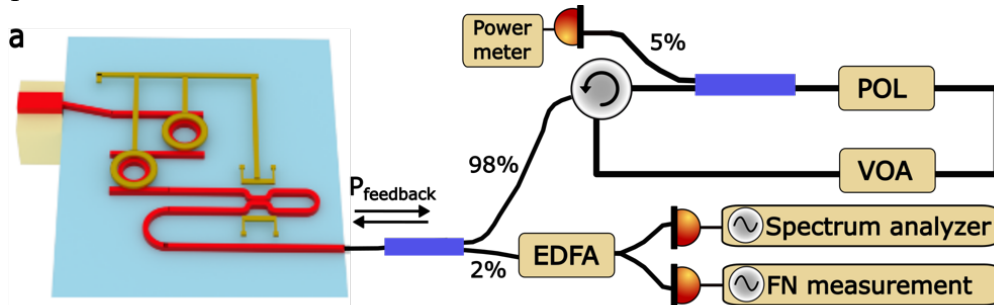


Supplementary Fig. 4 Additional free running and coil-locked ECTL frequency noise measurements. **a** FN measurements of the freerunning ECTL at various points across the tuning range plotted with the calculated TRN limit of the ECTL rings (black-dashed). **b** FN of the ECTL stabilized to the 10-m coil reference cavity at various points across the tuning range using two independent measurement techniques (stitched together at the black vertical line) and plotted with the calculated TRN limit of the 10-m coil (blue-dashed). **c** Measurement of relative intensity noise (RIN) of the ECTL at various points across the tuning range.

Supplementary Note 5: Laser feedback measurements

To directly measure the effect of optical feedback on our ECTL we designed an optical feedback setup, illustrated in Supplementary Fig. 5, where the ECTL output power is fed back to itself using

a fiber circulator and a variable optical attenuator (VOA) to control the optical feedback level. The full feedback circuit is on the order of 25 meters long. The power returned to the ECTL is monitored by tapping 5% of the feedback power and measuring on a power meter. The power returning to the PIC is polarization sensitive and must be adjusted to maximize the optical feedback before making any measurements. A small portion of the ECTL output is diverted to an EDFA and then to an OFD setup to measure the frequency noise of the laser at different feedback levels. All losses in the circuit must be accounted for to most accurately determine the actual feedback power to the laser. For a fiber-coupled ECTL output power of 2.4 mW the maximum estimated optical feedback power was 0.5 mW.



Supplementary Fig. 5 ECTL feedback measurement. a Schematic of the experimental setup for measuring the effect of optical feedback on the ECTL. The laser output power is initially split in two: the majority for feeding back to the laser and a small portion to measure the laser frequency noise (FN). A variable optical attenuator (VOA) sets the feedback power level that is monitored with a power meter. Polarization (POL) paddles ensure the returned optical field is aligned properly with the silicon nitride waveguide. The FN is measured with an optical frequency discriminator (OFD) and an optical spectrum analyzer monitors for the onset of coherence collapse.

Supplementary References

1. Liu, K. *et al.* Photonic circuits for laser stabilization with integrated ultra-high Q and Brillouin laser resonators. *APL Photonics* **7**, 096104 (2022).
2. Liu, K. *et al.* 36 Hz integral linewidth laser based on a photonic integrated 4.0 m coil resonator. *Optica* **9**, 770 (2022).
3. Liu, K. *et al.* Common cavity waveguide coil-resonator stabilized hybrid integrated WDM laser with 89 Hz integral linewidth. in *2024 Optical Fiber Communications Conference and Exhibition (OFC)* 1–3 (2024).
4. Gundavarapu, S. *et al.* Sub-hertz fundamental linewidth photonic integrated Brillouin laser. *Nature Photon* **13**, 60–67 (2019).
5. Chauhan, N. *et al.* Visible light photonic integrated Brillouin laser. *Nat Commun* **12**, 4685 (2021).